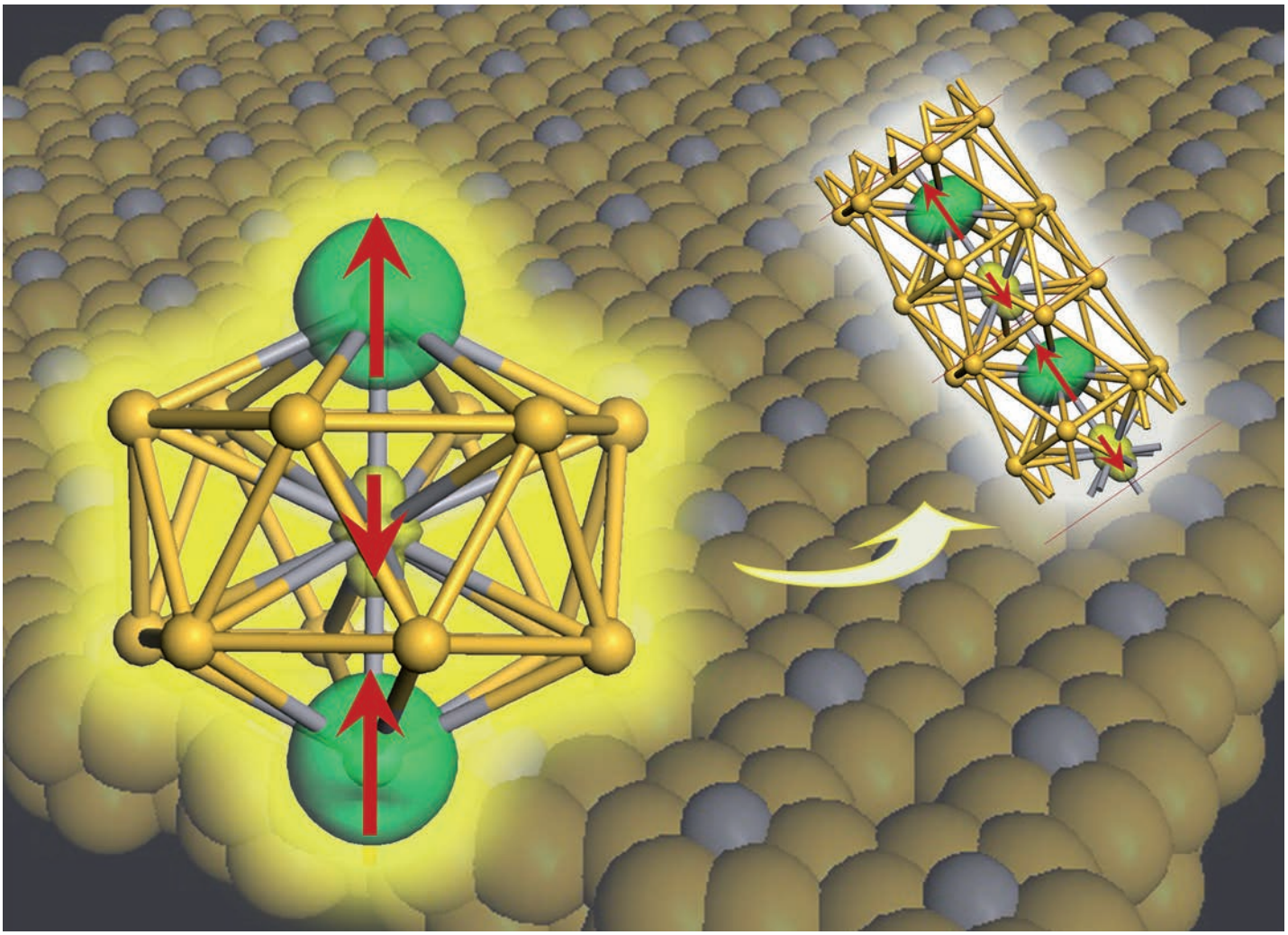

Showcasing research from Key Laboratory of Materials Modification by Laser, Ion and Electron Beams, Dalian University of Technology, China.

Discovery of a silicon-based ferrimagnetic wheel structure in $V_xSi_{12}^-$ (x = 1–3) clusters: photoelectron spectroscopy and density functional theory investigation

We investigated the ground state structures, electronic and magnetic properties of $V_xSi_{12}^-$ (x = 1–3) clusters using photoelectron spectroscopy combined with DFT-based genetic algorithm. $V_3Si_{12}^-$ has a bicapped hexagonal antiprism structure and exhibits ferromagnetic behavior with a total spin of 4 μ_B.

As featured in:

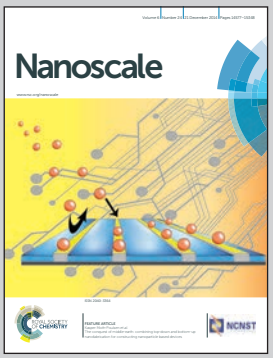

See Jijun Zhao, Weijun Zheng *et al*. *Nanoscale*, 2014, **6**, 14617.

ROYAL SOCIETY OF CHEMISTRY

www.rsc.org/nanoscale

Registered charity number: 207890

Nanoscale

COMMUNICATION

View Article Online
View Journal | View Issue

Cite this: *Nanoscale*, 2014, **6**, 14617

Received 7th June 2014,
Accepted 9th September 2014

DOI: 10.1039/c4nr03130j

www.rsc.org/nanoscale

Discovery of a silicon-based ferrimagnetic wheel structure in $V_xSi_{12}^-$ (x = 1–3) clusters: photoelectron spectroscopy and density functional theory investigation†

Xiaoming Huang,[a] Hong-Guang Xu,[b] Shengjie Lu,[b] Yan Su,[a] R. B. King,[c] Jijun Zhao*[a,d] and Weijun Zheng*[b]

Our studies show that VSi_{12}^- adopts a V-centered hexagonal prism with a singlet spin state. The addition of the second V atom leads to a capped hexagonal antiprism for $V_2Si_{12}^-$ in a doublet spin state. Most interestingly, $V_3Si_{12}^-$ exhibits a ferrimagnetic, bicapped hexagonal antiprism wheel-like structure with a total spin of $4\mu_B$.

Silicon is the backbone of the microelectronics industry. The miniaturization trend of electronic devices has motivated tremendous efforts for developing new silicon nanostructures[1] and for investigating silicon clusters.[2–5] Transition metal (TM)-doped silicon clusters are of particular interest because the TM dopants can not only stabilize the silicon clusters[6,7] but also introduce novel physical/chemical properties such as large HOMO–LUMO gaps,[8] high magnetic moments,[9] and tunable hyperpolarizability.[10] Moreover, these metal-encapsulating silicon clusters may act as building blocks in novel materials,[11,12] such as one-dimensional (1D) ferromagnetic nanotubes.[13–16]

Among the previous studies on the metal-doped silicon clusters, $TM@Si_{12}$ clusters have attracted significant attention.[6,10,14,17–23] Hiura *et al.*[6] reported the high stability of a WSi_{12} cluster, which possesses an endohedral tungsten atom in a silicon cage configuration, and it satisfies the 18-electron rule.[24,25] Sen and Mitas[26] systematically investigated the encapsulation of a TM atom (3d, 4d, and 5d series) inside a Si_{12} hexagonal prism cage and found the cage configuration to be remarkably stable regardless of the species of TM atom. Khanna and co-workers[17] found that the stability of $Cr@Si_{12}$ can be also explained by the 18-electron rule, and the large magnetic moment ($6\mu_B$) of the Cr atom is completely quenched by the Si_{12} hexagonal prism. In addition, they also explored the ground state geometries, electronic properties, and stabilities of the other $TM@Si_{12}$ (TM = Sc–Ni) clusters using density functional theory (DFT) calculations.[17,18]

To date, most of the experimental and theoretical studies were focused on silicon clusters doped with a single TM atom, whereas much less is known about silicon clusters with multiple TM dopants. Ji and Luo[27] investigated the geometries, magnetic properties and stabilities of a number of TM_2Si_{18} (TM = Ti, V, Cr, Mn, Fe, Co, Ni, Cu or Zn) clusters using DFT calculations. They found that the magnetic moments of these clusters are almost quenched, except that Mn_2Si_{18}, Fe_2Si_{18} and Cu_2Si_{18} are magnetic with the total moments of $2\mu_B$. A spin moment of $2\mu_B$ was also found in a hydrogenated $Cr_2Si_{18}H_{12}$ cluster.[28] Xu *et al.* used photoelectron spectroscopy and DFT to reveal strong V–V interaction and weak Sc–Sc interaction in the V_2Si_n [12,29] and Sc_2Si_n [30] clusters, respectively. Furthermore, they showed that the V_2Si_{20} cluster has a V_2 unit encapsulated inside an elongated dodecahedron Si_{20} cage structure.[12] Because the V–V interaction is very strong, it would be especially interesting to investigate change in the structures and properties of V-doped silicon clusters upon the incorporation of additional V atoms.

In this investigation, we report photoelectron spectroscopy and density functional theory studies of $V_xSi_{12}^-$ (x = 1, 2, 3) clusters, illustrating the effect of multiple TM atoms on the equilibrium structures of silicon frameworks, as well as the electronic and magnetic properties of the TM-Si binary clusters. Most impressively, we found that $V_3Si_{12}^-$ has a wheel-like bicapped hexagonal antiprism structure, and it is ferrimagnetic with a total magnetic moment of $4\mu_B$, making it a promising building block in nanoscale spintronics and high-density magnetic storage.

[a]*Key Laboratory of Materials Modification by Laser, Ion and Electron Beams, Dalian University of Technology, Ministry of Education, Dalian 116024, China. E-mail: zhaojj@dlut.edu.cn*
[b]*State Key Laboratory of Molecular Reaction Dynamics, Institute of Chemistry, Chinese Academy of Sciences, Beijing 100190, China. E-mail: zhengwj@iccas.ac.cn*
[c]*Department of Chemistry and Center for Computational Chemistry, University of Georgia, Athens, Georgia, USA*
[d]*Beijing Computational Science Research Center, Beijing 100089, China*

†Electronic supplementary information (ESI) available: Cartesian coordinates, on-site charge, spin, and bond lengths, plots of low-energy isomer structures for $V_xSi_{12}^-$ (x = 1, 2, 3) clusters. Spatial distribution of molecular orbitals for VSi_{12}^- cluster, energies of molecular orbitals for V_3Si_{12} and $V_3Si_{12}^-$ clusters. Comparison of VDEs and photoelectron spectra simulated by PBE, RPBE, M06, M06-L functionals and experiments. See DOI: 10.1039/c4nr03130j

The lowest-energy configurations of $V_xSi_{12}^-$ (x = 1, 2, 3) clusters from GA-DFT global optimizations are shown in Fig. 1. The structures of some low-lying isomers are given in Fig. S1 of the ESI.† For each anionic cluster, we computed the vertical detachment energy (VDE) and adiabatic detachment energy (ADE). The binding energies, VDEs, ADEs, and total magnetic moments of these three clusters are summarized in Table 1. Based on the ground state geometries, the photoelectron spectra of $V_xSi_{12}^-$ (x = 1, 2, 3) cluster anions are simulated using the PBE/DND scheme and compared with the experimental spectra in Fig. 2. The VDEs and ADEs from theoretical calculations are very close to the experimental values with average deviations of ~0.1 eV. The experimental photoelectron spectra of V_xSi_{12} cluster anions are also well reproduced by the theoretical calculations. The excellent agreements clearly indicate that our GA-DFT global search has located the true ground state configurations of the $V_xSi_{12}^-$ (x = 1, 2, 3) clusters, and that our PBE/DND scheme is able to describe the electronic states of these clusters to a satisfactory extent.

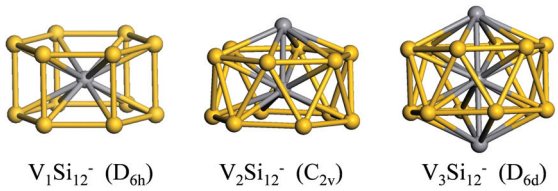

Fig. 1 Ground state structures of $V_xSi_{12}^-$ (x = 1, 2, 3) clusters.

Table 1 Binding energy (E_b), VDE, ADE, and total magnetic moments of $V_xSi_{12}^-$ (x = 1, 2, 3) clusters (unless specified with "Expt.", all values are from DFT calculations)

Cluster	E_b (eV per atom)	VDE (eV)		ADE (eV)		Spin (μ_B)
		Expt.	Theo.	Expt.	Theo.	
VSi_{12}^-	4.09	3.82 ± 0.08	3.94	3.71 ± 0.08	3.87	0
$V_2Si_{12}^-$	4.12	3.66 ± 0.08	3.75	3.55 ± 0.08	3.69	1
$V_3Si_{12}^-$	4.13	2.59 ± 0.08	2.54	2.44 ± 0.08	2.53	4

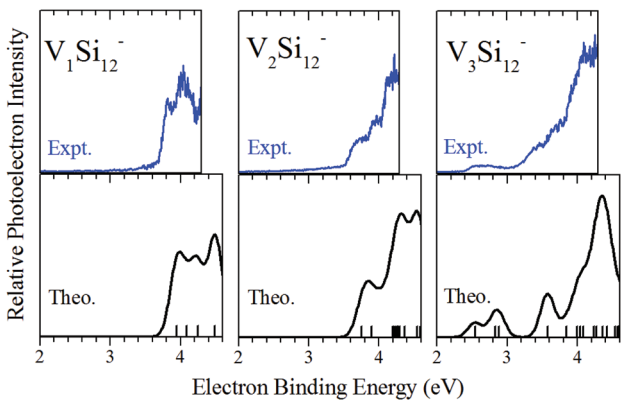

Fig. 2 Photoelectron spectra of $V_xSi_{12}^-$ (x = 1, 2, 3) clusters. Upper: experiment; lower: theoretical simulation. In the theoretical spectra, a uniform Gaussian broadening of 0.1 eV is chosen, and the energy levels of clusters from DFT calculations are labelled by short vertical lines.

As shown in Fig. 1, VSi_{12}^- adopts a hexagonal prism cage (D_{6h}) with an endohedral V atom. This is in agreement with the structures of the neutral VSi_{12} [14,26] and the VSi_{12}^- anion[18] found by the previous DFT calculations, as well as the distorted hexagonal prism structure of the VSi_{12}^+ cation found by infrared multiple photon dissociation spectroscopy.[31] Moreover, VSi_{12}^- possesses a closed shell electronic configuration with a large HOMO–LUMO gap of 2.01 eV, obeying the 18-electron rule.[17,18,26] Indeed, the spatial distributions of molecular orbitals exhibit the distinct feature of a $1S^21P^61D^{10}$ electron shell (Fig. S2†). Similar to its isoelectronic counterpart $CrSi_{12}$,[17,26] the VSi_{12}^- cluster is entirely non-magnetic. The previous DFT calculations[18,26] predicted that the ground state of $TM@Si_{12}$ clusters for the 3d TM series usually has the lowest spin multiplicity, *i.e.*, singlet for the even numbers of electrons and doublet for the odd numbers of electrons.

Incorporation of another vanadium atom into VSi_{12}^- transforms the hexagonal prism cage of the Si_{12} skeleton into a distorted Si_{12} hexagonal antiprism with C_{2v} symmetry, with the second V atom capping one of the hexagonal faces of the antiprism. Because of the strong V–V interaction,[12,29] the two V atoms in $V_2Si_{12}^-$ cluster tend to stay together. Note that the isomer with two separated V atoms (isomer d in Fig. S1†) is energetically less favorable by 1.67 eV. Similar to VSi_{12}^-, $V_2Si_{12}^-$ still adopts the lowest spin multiplicity (doublet state).

Further addition of the third V atom leads to a bicapped hexagonal antiprism (D_{6d}). This can be viewed as a wheel structure, in which three V atoms form a central axle surrounded by the Si_{12} hexagonal antiprism. A similar D_{6h} wheel structure with a Si_{12} hexagonal prism rather than an antiprism (isomer d in Fig. S1†) is found to be less stable by 0.912 eV. Clearly, the incorporation of multiple V atoms has a pronounced effect on the geometry of the Si_{12} frame. More impressively, the magnetism of V atoms is partially recovered after the inclusion of the third V atom. According to our spin-polarized DFT calculations, the doping of three V atoms into a Si_{12} cluster leads to a total magnetic moment of $4\mu_B$ and $3\mu_B$ for the anionic and neutral clusters, respectively.

The magnetic moments of the neutral and anionic V_3Si_{12} clusters can be interpreted by the Wade–Mingos rules,[32,33] which historically were derived to relate the structures of polyhedral boranes to the number of skeletal electrons. Later, they were used to explain the shapes of other clusters that are isoelectronic and isolobal with boranes.[34] According to the Wade–Mingos rules, $2n + 2$ electrons are needed for skeletal bonding in a deltahedron with n vertices, where a deltahedron is defined as a polyhedron with all triangular faces. Normally, counting skeletal electrons by the Wade–Mingos rules assumes that each vertex atom uses three valence orbitals for skeletal bonding, leaving the remaining orbitals for bonding to external groups or for lone pairs. In the case of V_3Si_{12}, the interior V atom contributes all of its five valence electrons, and the surface V atoms can be assumed to use a six-orbital sd^5 manifold because the 4p orbitals are significantly high in

energy for its valence orbital manifold. This leaves three external orbitals to accommodate the five valence electrons of each surface V atom. One of these external orbitals thus has an unpaired electron, which contributes to the overall spin of the cluster. As a consequence, the surface V atoms do not contribute any electrons to the skeletal bonding.

In counting skeletal electrons in V_3Si_{12}, each silicon atom contributes two skeletal electrons, leaving an external lone pair. These two skeletal electrons for each silicon atom, combined with the five skeletal electrons from the central vanadium atom, leads to a total of $12 \times 2 + 5 = 29$ skeletal electrons corresponding to one hole, *i.e.*, one unpaired electron in the 30 skeletal electron closed-shell configuration for a 14-vertex bicapped square antiprism. This hole, along with the two unpaired electrons from the two surface vanadium atoms, result in a total of three unpaired electrons in the neutral V_3Si_{12}, corresponding to a magnetic moment of $3\mu_B$. The extra electron in the $V_3Si_{12}^-$ anion does not pair up with any of these unpaired electrons instead increases the total magnetic moment to $4\mu_B$.

Furthermore, the population analysis of $V_3Si_{12}^-$ (Table S1†) shows that the alignment of local magnetic moments on V atoms is ferrimagnetic with $+2.4\mu_B$ on each of the surface V atoms and $-0.6\mu_B$ on the interior V atom. The magnitude of the on-site moment of the interior V atom is about 1/4 fold of that of surface V atom and non-negligible. There are also small and negligibly induced moments on Si atoms ($-0.018\mu_B$ on average). Intuitively, the ferrimagnetism of $V_3Si_{12}^-$ can be attributed to the different coordination numbers (CN) of the interior V atom (CN = 14) and the surface V atoms (CN = 7), as well as the different V–Si bond lengths, *i.e.*, 2.682 Å for the interior V atom and 2.707 Å for the surface V atoms (Table S2†). It is known that reduced CN and elongated interatomic distance can result in an enhanced local magnetic moment on the TM atom in a cluster.[35]

The interactions between Si and V atoms can be further analyzed by the partial density of p and d states, shown in Fig. 3 (contribution from s states is negligible, and thus not shown). It is known that p–d hybridization and Si-to-metal charge transfer are the two important factors for the quenching of the local magnetic moment of the TM atom in a metal-doped silicon cluster.[15,16,26] From Fig. 3, it can be observed that the interior V atom has stronger p–d hybridization with the surrounding Si atoms than with the surface V atom. The local magnetic moment of $+2.4\mu_B$ on each surface V atom mainly originates from the d states of the majority spin near the Fermi level, which only slightly hybridize with the p states of the Si atoms. In addition, the negative moment of $-0.6\mu_B$ on the interior V atom can be related to the peak of d states of the minority spin located ~1 eV below the Fermi level, which does not overlap with the p states of Si atoms. On-site Mulliken population analysis (Table S1†) also shows that the interior V atom gains 0.64 electrons from the surrounding Si atoms, while the surface V atom gains only about 0.09 electrons.

As shown in Fig. 4, the hexagonal antiprism of V_3Si_{12} may further act as building blocks for novel 1D V-centered Si nanowire, similar to the previous cases of $TM@Si_{12}$ and $TM@Si_{10}$ clusters.[13–16] Our spin-polarized DFT calculations show that the assembled nanowire is still ferrimagnetic, *i.e.*, one V atom with spin moment of $1.076\mu_B$, and another with a moment of $-0.181\mu_B$. Previously, ferrimagnetic clusters were mainly observed in small transition metal oxide systems such as Fe_4O_6,[36] Mn_3O^-, $Mn_3O_2^-$, and Mn_4O^-.[37] Considering the advantage of the mature silicon-based microelectronic technology, the discovery of Si-based ferrimagnetic clusters (and possibly, 1D nanowire) is rather tempting for the future spintronic applications,[38] such as spin filters,[39] exchange bias[40] and spin-resolved light-emitting diodes (spin-LEDs).[41] In the cluster assemblies, it might be possible to retain the negative charge on the $V_3Si_{12}^-$ cluster by appropriately combining with the elements of low electron affinity (*e.g.*, alkali metals), like the cluster-assembled ionic solids of $K(Al_{13})$[42] and $Cs(BAl_{12})$.[43]

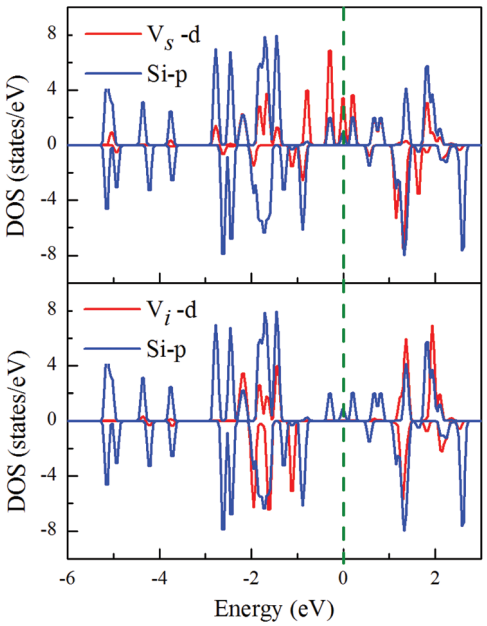

Fig. 3 Partial density of states (DOS) for $V_3Si_{12}^-$ cluster. Blue curves denote p orbitals of six Si atoms belonging to the same layer of the antiprism, and red curves are the d orbitals of one V atom (upper for the surface V_s atom bonded with the six Si atoms, and lower for the interior V_i atom). Green dashed line is the Fermi level.

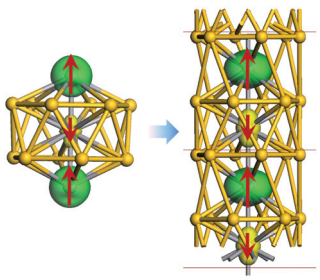

Fig. 4 Geometries and isosurfaces of spin densities (green for majority spin and yellow for minority spin) for $V_3Si_{12}^-$ cluster (left) and $(V_2Si_{12})_n$ nanowire (right).

To summarize, the incorporation of more than one V atom in the Si_{12} host cluster not only modifies the equilibrium geometry, but also partially recovers the magnetic moments of the V atoms. Combining anion photoelectron spectroscopy and a DFT-based global search, $V_3Si_{12}^-$ cluster is shown to possess a bicapped hexagonal antiprism structure with a ferrimagnetic alignment of local moments on the interior and surface V atoms. The Wade–Mingos rules are able to explain the four unpaired electrons in the 14-vertex deltahedron of $V_3Si_{12}^-$. The different local magnetic moments on V atoms are attributed to different p–d hybridizations between the V and Si atoms. This ferrimagnetic $V_3Si_{12}^-$ (or V_3Si_{12}) cluster with high spin multiplicity is expected to be useful in future nanoscale magnetic materials and spintronic devices. Moreover, the present results suggest new opportunities in tailoring the electronic and magnetic properties of doped silicon clusters by varying the number and composition of transition metal dopants.

Methods

The experiments were conducted on a previously described[30] home-built apparatus consisting of a laser vaporization source, a time-of-flight (TOF) mass spectrometer, and a magnetic-bottle photoelectron spectrometer. The V–Si cluster anions were generated in the laser vaporization source by the laser ablation of a rotating translating disk target (13 mm in diameter, V/Si mole ratio 1 : 2) with a nanosecond Nd:YAG laser (Continuum Surelite II-10). Helium gas with ~4 atm backing pressure was allowed to expand through a pulsed valve (General Valve Series 9) into the source to cool the formed clusters. The generated cluster anions were mass-analyzed with the TOF mass spectrometer. The $V_xSi_{12}^-$ (x = 1, 2, 3) clusters were individually selected with a mass gate, decelerated by a momentum decelerator, and crossed with a beam of an Nd:YAG laser (Continuum Surelite II-10, 266 nm) in the photodetachment region. The electrons from photodetachment were energy-analyzed by the magnetic bottle photoelectron spectrometer; the resolution of the photoelectron spectrometer was about ~40 meV for electrons with 1 eV kinetic energy.

To determine the lowest-energy structures of $V_xSi_{12}^-$ (x = 1, 2, 3) clusters, an unbiased global search was performed using a genetic algorithm (GA)[44,45] incorporated with DFT. The details of this GA-DFT scheme can be found in our previous publication.[46] For each cluster, sixteen random configurations were generated from the beginning as the initial GA population. The GA search was continued for at least 1000 iterations to ensure the global minimum structure. *Ab initio* calculations were performed using the spin-polarized all-electron DFT as implemented in the DMol^3 program.[47] The generalized gradient approximation (GGA) with PBE parameterization[48] was adopted to describe the exchange-correlation interaction. A double numerical basis set including d-polarization functions (DND) was employed. Vibrational analyses were performed to ensure that the optimized structures are the true minima on the potential energy surface.

By definition, VDE is the energy difference between the anion and the neutral cluster, with the latter fixed at the anion geometry; AEA is the energy difference between the anionic and neutral clusters in their optimized lowest-energy configurations. For all the calculations, only the ground-state electron configurations were involved, and no excited state has been considered. All of the VDE and AEA values were computed by the difference of total energies from DFT calculations. Based on the energy levels of anionic clusters, photoelectron spectra were simulated using the generalized Koopmans' theorem (GKT), which has been previously described.[49] In the simulated DOS spectra, the peak of each transition corresponds to the removal of an electron from a specific molecular orbital of the cluster anion. During the simulation, the relative energies of the orbitals (ΔE_n) were calculated by the equation: $\Delta E_n = E_{(\mathrm{HOMO}-n)} - E_{\mathrm{HOMO}}$, where $E_{(\mathrm{HOMO}-n)}$ is the energy of the (HOMO−n) orbital from theoretical calculations, E_{HOMO} is the energy of the HOMO, and ΔE_n is the relative energies of the (HOMO−n) orbital with regard to the HOMO. The peak associated with the HOMO was set to the position of calculated VDE of each isomer, and the peaks of the deeper orbitals were shifted according to their relative energies, compared to the HOMO.

It is suspected that the conventional GGA with PBE parameterization might not be very reliable for describing transition-metal systems with spin polarization.[50] Therefore, RPBE,[51] M06-L,[52] and M06 functionals[53] (which have been recommended for transition metals[54]) have been applied to compute the VDEs and to simulate the photoelectron spectra of the V_xSi_{12} cluster anions. The results are provided in Table S4 and Fig. S4 of the ESI,† respectively. Clearly, all four functionals (PBE, RPBE, M06 and M06-L) are able to reasonably reproduce the experimental VDEs, with an average deviation between 0.05 and 0.09 eV. With the same PBE functional, the choice of the basis sets has only minor influence on the computed VDE values. Similar coincidences are found in the simulated photoelectron spectra by the different methods (Fig. S4†). Therefore, the present choice of PBE/DND scheme is supported by the other functionals and basis sets.

Acknowledgements

This work was supported by the National Natural Science Foundation of China (no. 11134005, 11304030, and 21103202), the Fundamental Research Funds for the Central Universities of China (no. DUT14LK19, DUT13ZD207), and the Knowledge Innovation Program of the Chinese Academy of Sciences (no. KJCX2-EW-H01). The authors thank Prof. Jun Li and Prof. Ling Jiang for valuable discussions.

Notes and references

1 V. Kumar, *Nanosilicon*, Elsevier, 2011.
2 X. Zhu and X. C. Zeng, *J. Chem. Phys.*, 2003, **118**, 3558.

3 X. L. Zhu, X. C. Zeng, Y. A. Lei and B. Pan, *J. Chem. Phys.*, 2004, **120**, 8985.
4 S. Yoo and X. C. Zeng, *J. Chem. Phys.*, 2006, **124**, 054304.
5 S. Yoo, J. Zhao, J. Wang and X. C. Zeng, *J. Am. Chem. Soc.*, 2004, **126**, 13845–13849.
6 H. Hiura, T. Miyazaki and T. Kanayama, *Phys. Rev. Lett.*, 2001, **86**, 1733–1736.
7 Y. Gao and X. C. Zeng, *J. Chem. Phys.*, 2005, **123**, 204325.
8 V. Kumar and Y. Kawazoe, *Phys. Rev. Lett.*, 2001, **87**, 045503.
9 V. T. Ngan, E. Janssens, P. Claes, J. T. Lyon, A. Fielicke, M. T. Nguyen and P. Lievens, *Chem. – Eur. J.*, 2012, **18**, 15788–15793.
10 J. He, K. Wu, R. Sa, Q. Li and Y. Wei, *Chem. Phys. Lett.*, 2010, **490**, 132–137.
11 V. Kumar, *Comput. Mater. Sci.*, 2006, **36**, 1–11.
12 H.-G. Xu, X.-Y. Kong, X.-J. Deng, Z.-G. Zhang and W.-J. Zheng, *J. Chem. Phys.*, 2014, **140**, 024308.
13 A. K. Singh, T. M. Briere, V. Kumar and Y. Kawazoe, *Phys. Rev. Lett.*, 2003, **91**, 146802.
14 N. A. Antonis, M. Giannis, E. F. George and M. Madhu, *New J. Phys.*, 2002, **4**, 78.
15 L. Ma, J. Zhao, J. Wang, B. Wang, Q. Lu and G. Wang, *Phys. Rev. B: Condens. Matter*, 2006, **73**, 125439.
16 J. Wang, J. Zhao, L. Ma, G. Wang and R. B. King, *Nanotechnology*, 2007, **18**, 235705.
17 S. N. Khanna, B. K. Rao and P. Jena, *Phys. Rev. Lett.*, 2002, **89**, 016803.
18 J. U. Reveles and S. Khanna, *Phys. Rev. B: Condens. Matter*, 2005, **72**, 165413.
19 N. Uchida, T. Miyazaki and T. Kanayama, *Phys. Rev. B: Condens. Matter*, 2006, **74**, 205427.
20 J. Lu and S. Nagase, *Phys. Rev. Lett.*, 2003, **90**, 115506.
21 W. J. Zheng, J. M. Nilles, D. Radisic and K. H. Bowen, *J. Chem. Phys.*, 2005, **122**, 071101.
22 X. Y. Kong, H.-G. Xu and W. J. Zheng, *J. Chem. Phys.*, 2012, **137**, 064307.
23 H.-G. Xu, M. M. Wu, Z.-G. Zhang, J.-Y. Yuan, Q. Sun and W.-J. Zheng, *J. Chem. Phys.*, 2012, **136**, 104308.
24 I. Langmuir, *Science*, 1921, **54**, 59–67.
25 P. Pyykkö, *J. Organomet. Chem.*, 2006, **691**, 4336–4340.
26 P. Sen and L. Mitas, *Phys. Rev. B: Condens. Matter*, 2003, **68**, 155404.
27 W. Ji and C. Luo, *Int. J. Quantum Chem.*, 2012, **112**, 2525–2531.
28 V. Kumar and Y. Kawazoe, *Phys. Rev. Lett.*, 2003, **90**, 055502.
29 H.-G. Xu, Z.-G. Zhang, Y. Feng, J. Yuan, Y. Zhao and W. Zheng, *Chem. Phys. Lett.*, 2010, **487**, 204–208.
30 H.-G. Xu, Z.-G. Zhang, Y. Feng and W. Zheng, *Chem. Phys. Lett.*, 2010, **498**, 22–26.
31 P. Claes, E. Janssens, V. T. Ngan, P. Gruene, J. T. Lyon, D. J. Harding, A. Fielicke, M. T. Nguyen and P. Lievens, *Phys. Rev. Lett.*, 2011, **107**, 173401.
32 K. Wade, *Chem. Soc. D*, 1971, 792–793.
33 D. M. P. Mingos, *Acc. Chem. Res.*, 1984, **17**, 311–319.
34 R. King, I. Silaghi-Dumitrescu and M. Ută, *J. Chem. Theor. Comput.*, 2008, **4**, 209–215.
35 F. Liu, M. R. Press, S. N. Khanna and P. Jena, *Phys. Rev. B: Condens. Matter*, 1989, **39**, 6914–6924.
36 A. Kirilyuk, A. Fielicke, K. Demyk, G. von Helden, G. Meijer and T. Rasing, *Phys. Rev. B: Condens. Matter*, 2010, **82**, 020405.
37 K. S. Williams, J. P. Hooper, J. M. Horn, J. M. Lightstone, H. Wang, Y. J. Ko and K. H. Bowen, *J. Chem. Phys.*, 2012, **136**, 134315.
38 C. Felser and G. H. Fecher, *Spintronics: From Materials to Devices*, Springer, 2013.
39 J. S. Moodera, T. S. Santos and T. Nagahama, *J. Phys.: Condens. Matter*, 2007, **19**, 165202.
40 F. Radu, R. Abrudan, I. Radu, D. Schmitz and H. Zabel, *Nat. Commun.*, 2012, **3**, 715.
41 L. Fang, K. D. Bozdag, C.-Y. Chen, P. Truitt, A. Epstein and E. Johnston-Halperin, *Phys. Rev. Lett.*, 2011, **106**, 156602.
42 F. Liu, M. Mostoller, T. Kaplan, S. N. Khanna and P. Jena, *Chem. Phys. Lett.*, 1996, **248**, 213.
43 C. Ashman, S. N. Khanna, F. Liu, P. Jena, T. Kaplan and M. Mostoller, *Phys. Rev. B: Condens. Matter*, 1997, **55**, 15868.
44 R. L. Johnston, *Dalton Trans.*, 2003, 4193–4207.
45 J. Zhao and R.-H. Xie, *J. Comput. Theor. Nanosci.*, 2004, **1**, 117–131.
46 L. Sai, L. Tang, J. Zhao, J. Wang and V. Kumar, *J. Chem. Phys.*, 2011, **135**, 184305.
47 B. Delley, *J. Chem. Phys.*, 2000, **113**, 7756–7764.
48 J. P. Perdew, K. Burke and M. Ernzerhof, *Phys. Rev. Lett.*, 1996, **77**, 3865.
49 J. Akola, M. Manninen, H. Häkkinen, U. Landman, X. Li and L.-S. Wang, *Phys. Rev. B: Condens. Matter*, 1999, **60**, R11297.
50 A. J. Cohen, P. Mori-Sanchez and W. Yang, *Science*, 2008, **321**, 792–794.
51 B. Hammer, L. B. Hansen and J. K. Nørskov, *Phys. Rev. B: Condens. Matter*, 1999, **59**, 7413–7421.
52 Y. Zhao and D. G. Truhlar, *J. Chem. Phys.*, 2006, **125**, 194101.
53 Y. Zhao and D. G. Truhlar, *Theor. Chem. Acc.*, 2008, **120**, 215–241.
54 S. Luo, B. Averkiev, K. R. Yang, X. Xu and D. G. Truhlar, *J. Chem. Theory Comput.*, 2014, **10**, 102.